ACS OMEGA

http://pubs.acs.org/journal/acsodf

Article

Electronic Structure Calculations of Static Hyper(Polarizabilities) of Substrate-Supported Group-IV and -V Elemental Monolayers

Sumandeep Kaur, Ravindra Pandey,* and Shashi P. Karna*

Cite This: *ACS Omega* 2023, 8, 9614−9620

Read Online

ACCESS | Metrics & More | Article Recommendations | Supporting Information

ABSTRACT: The substrate-induced effects on the polarizability (α) and first dipole hyperpolarizability (β) of group-IV (i.e., graphene, silicene, germanene, stanene) and group-V (i.e., phosphorene, arsenene, antimonene, and bismuthene) elemental monolayer nanoflakes are investigated. Density functional theory calculations show that these monolayers are bound with varying degrees of interaction strength with the Ag(111) substrate surface. Calculated dipole moment and β values are zero for the centrosymmetric configurations of the pristine elemental monolayers. On the other hand, substrate-induced changes in the electronic densities at the interface lead to substantially enhanced values of β, making these materials attractive for applications in the next-generation photonic technologies at the nanoscale.

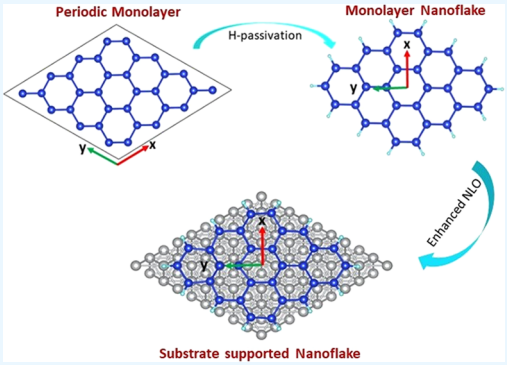

1. INTRODUCTION

Materials exhibiting nonlinear optical (NLO) properties have important applications in a wide range of emerging technologies in photonics, including on-chip nanophotonics, nonlinear plasmonics, and quantum nanophotonics.[1,2] Among the current NLO materials, silica fibers, $LiNbO_3$, and β-$BaBiO_3$ are widely used due to their high efficiency and enhanced environmental stability. However, these materials present challenges in processing, fabrication, and integration with other materials.[3] Due to this, there is an intense interest in developing materials with enhanced NLO response and ease in fabrication and integration with other materials. This has attracted a great deal of interest in two-dimensional (2D) nanomaterials, which in addition to exhibiting ultrafast NLO response, also possess other electronic, geometrical, and chemical properties that are highly desirable for future photonics and optoelectronics technologies.[4−7]

The phase-matching condition is another advantage of 2D materials for solid-state photonics applications. In general, nonlinear effects in crystals and bulk phases occur when the phase-matching condition (i.e., the photon's momentum and energy are simultaneously conserved before and after the nonlinear process) is satisfied. This, in turn, requires a careful design of the incident light path and the crystal's orientation to optimize the crystal's nonlinear responses. In the case of 2D material, a medium with a reduced thickness that is comparable to the sub-wavelength range and shorter than the coherence length, the phase-matching condition can be easily achieved relative to their bulk counterparts.[8−10]

Free-standing elemental 2D materials have zero dipole and first-order NLO response due to centrosymmetric configuration. However, when deposited on a hetero-substrate, the centrosymmetry is lifted. Substrate-supported 2D monolayers also exhibit changes in electronic density due to interaction with the former. Both these effects are expected to lead to measurable dipole moment and NLO susceptibilities. To examine this hypothesis and understand the evolution of NLO properties of elemental 2D materials, we have calculated the polarizability (α) and first-hyperpolarizability (β) of the Ag(111) substrate-supported graphene silicene,[11−15] germanene,[16] stanene,[17] phosphorene,[18] arsenene,[19] antimonene[20] and bismuthine.[21] All considered 2D monolayers, except graphene and bismuthine, have been grown epitaxially on Ag(111) substrate, which offers a good lattice (hexagonal) for the growth of honeycomb-like monolayers.[11−24]

2. COMPUTATIONAL METHOD

Computations were performed in a two-step approach: (i) first-principles density functional theory (DFT) calculations were performed on the pristine monolayers and their substrate-supported configurations to obtain electronic and geometrical structures and substrate−2D monolayer interaction energy; (ii) the semiempirical quantum-chemical coupled perturbed Hartree−Fock method as implemented in the semiempirical PM7 model (CPHF-PM7)[25,26] calculations were performed to

Received: January 13, 2023
Accepted: January 30, 2023
Published: February 28, 2023

https://doi.org/10.1021/acsomega.3c00232
ACS Omega 2023, 8, 9614−9620

obtain dipole moment, and (hyper)polarizabilities at the DFT-optimized equilibrium geometries. The use of the semi-empirical method for NLO property calculations in this work was dictated by the computational complexities of the system considered. To assess the accuracy of the CPHF-PM7 results, the results were benchmarked by comparing them with the CPHF-DFT results for the pristine nanoflakes.[27]

The periodic DFT calculations were performed employing the Vienna Ab initio Simulation Package (VASP).[28] The electron exchange and correlation functional forms were treated within the framework of generalized gradient approximation using the Perdew−Burke−Ernzerhof (PBE) functional form. The projector augmented wave method was used to describe electron−ion interaction,[29] and contributions from the van der Waals (vdW) interactions were incorporated using the D2 term of Grimme.[30] A plane-wave basis set with a kinetic energy cutoff of 520 eV together with (5 × 5 × 1) *k*-point mesh was used. A vacuum of about 15 Å along the *z*-direction in the periodic supercell was also used perpendicular to the plane of the monolayer. The structures were fully relaxed with residual forces smaller than 0.01 eV/Å on each atom. The energy convergence value between two consecutive steps was 10^{-5} eV. A three-layer periodic slab model was used to represent the Ag(111) substrate in the substrate-supported periodic calculations.[31,32]

The PM7 calculations based on the time-dependent coupled perturbed Hartree−Fock method[33] were performed using the Gaussian 16 program package[34] with the convergence criteria for the RMS density matrix, and changes in total energy were set at 10^{-8} and 10^{-6} eV, respectively. A finite cluster model consisting of fragments of the periodic configurations (referred to as monolayer nanoflakes) was used to calculate NLO properties.

Briefly, the linear polarizability is calculated as

$$\langle\alpha\rangle = \frac{1}{3}(\alpha_{xx} + \alpha_{yy} + \alpha_{zz}) \quad (1)$$

while the first-order dipole hyperpolarizability (β) is calculated as

$$\beta = (\beta_x^2 + \beta_y^2 + \beta_z^2)^{1/2} \quad (2)$$

which corresponds to the static β (0; 0, 0) effect.

Previously, β values obtained by the PM7 model were benchmarked for molecules, such as benzene and CO_2, and also for the organic molecules, including the three fluorenyl derivatives, namely, 7-nitro-9*H*-fluoren-2-ylamine, 1-(7-nitro-9*H*-fluoren-2-yl)-pyrrolidine, and [2-(7-nitro-9*H*-fluoren-2-yl)-vinyl]-1-1′-dipyrrolidine. It was concluded that the PM7 model gives accurate results comparable to DFT for small organic molecules, while the accuracy depends on the symmetry of large organic molecules.[35,36] We note that the parameterizations and approximations of semiempirical methods limit its accuracy. Nevertheless, at the same time, they increase their computational efficiency several times compared to the first-principles DFT methods. Therefore, semiempirical methods have constantly been employed to model the linear and nonlinear optical properties of molecular and low-dimensional materials.[35,36] We performed additional DFT calculations on pristine monolayer nanoflakes to benchmark the PM7 results. Overall, both the linear and NLO responses of the pristine nanoflakes were calculated using the DFT (PBE + D2/LANL2DZ) and PM7 levels of theory. On the other hand, we have only used the PM7 level of theory to calculate the linear and NLO responses of the substrate-supported monolayer nanoflakes.

3. RESULTS AND DISCUSSION

3.1. Structure and Stability. In the following, we present the periodic DFT results on the structural properties of the pristine and substrate-supported monolayers and the interaction energy between monolayer and substrate, Ag(111).

3.1.1. Pristine Monolayers. Figure 1 shows the graphene-like honeycomb structures of the elemental monolayers of group IV (graphene, silicene, germanene, stanene) and group V (phosphorene, arsenene, antimonene, and bismuthine) of the periodic table. The calculated structural properties listed in Table S1 (Supporting Information) are in excellent agreement with previously reported DFT studies.[37−45] Note that the D2 correction term decreases the lattice constant calculated using DFT.[41]

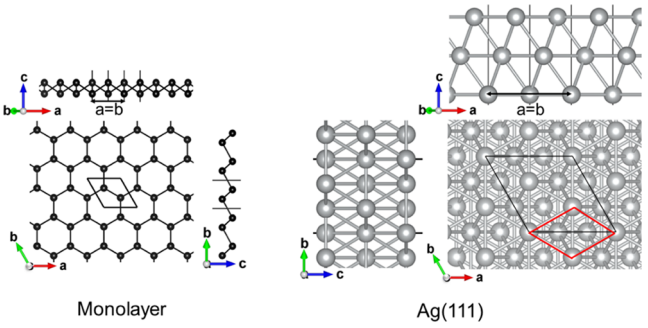

Figure 1. Top and side views of a monolayer and Ag(111) substrate. Red lines represent the primitive rhombus unit cell of the substrate.

3.1.2. Substrate-Supported Monolayers. For the periodic DFT calculations, the Ag(111) substrate was simulated in a slab model consisting of three layers with the $\sqrt{3} \times \sqrt{3}\ R\ 30°$ primitive unit cell, as displayed in Figure 1. The calculated lattice constant of Ag(111) is 4.24 Å, and the Ag−Ag distance is 2.99 Å. Figure 2 displays the substrate-supported monolayer configurations, which were constructed to keep lattice mismatch between monolayer and substrate at the minimum. For example, a honeycomb structure with the planar configuration for graphene and antimonene was considered, while the zigzag-buckled configurations were considered for the rest of the elemental monolayers. The considered periodic cell (*x*/*y*) configurations were $(4 \times 4/2\sqrt{3} \times \sqrt{3}\ R\ 30°)$ for C/Ag(111), $(4 \times 4/3\sqrt{3} \times \sqrt{3}\ R\ 30°)$ for Si/Ag(111), $(4 \times 4/3\sqrt{3} \times \sqrt{3}\ R\ 30°)$ for Ge/Ag(111), (2 × 2/3 × 3) for Sn/Ag(111), $(3 \times 3/2\sqrt{3} \times \sqrt{3}\ R\ 30°)$ for P/Ag(111), $(3 \times 3/2\sqrt{3} \times \sqrt{3}\ R\ 30°)$ for As/Ag(111), $(1 \times 1/1\sqrt{3} \times \sqrt{3}\ R\ 30°)$ for Sb/Ag(111), and (3 × 3/4 × 4) for Bi/Ag(111) (Table 1).[11−24]

Table 1 lists the details of the equilibrium configurations of the substrate-supported monolayers obtained at the PBE + D2 level of theory. We note that our choice of periodic supercell construction has introduced a lattice mismatch of 1−5% between the monolayers and the substrate, as listed in Table 1. The two planar monolayers, graphene and antimonene, exhibit quite a large lattice mismatch of 4.8 and 4.1%, respectively. The lattice-mismatch-induced strain is tensile except for germanene and arsenene, which experience a compressive strain in the substrate-supported configurations. Note that the

https://doi.org/10.1021/acsomega.3c00232
ACS Omega 2023, 8, 9614−9620

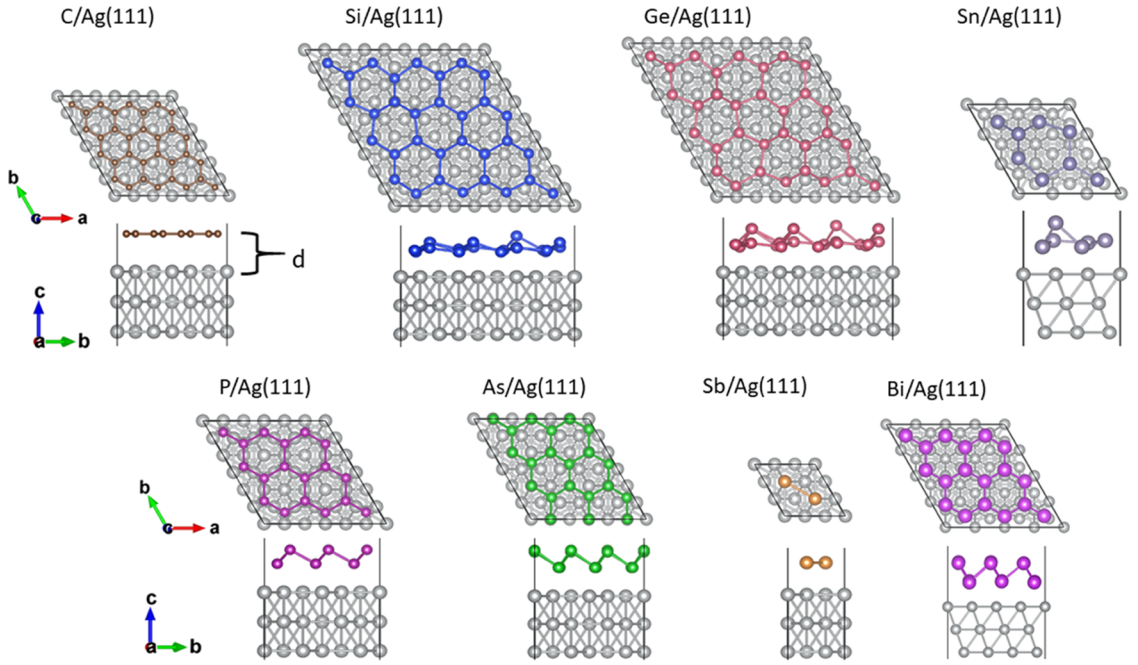

Figure 2. Top and side views of the equilibrium configurations of the Ag(111) substrate-supported monolayers. The interlayer distance is displayed by *d*. C, Si, Ge, Sn, P, As, Sb, and Bi represent graphene, silicene, germanene, stanene, phosphorene, arsenene, antimonene, and bismuthene, respectively.

Table 1. Equilibrium Configurations of the Ag(111) Substrate-Supported Monolayers Obtained at the PBE + D2 Level of Theory: Lattice Mismatch (%), Interlayer Distance (Å), and Interlayer Binding Energy (eV/atom)

	Ag(111) substrate-supported monolayers				
		periodic configurations (monolayer/substrate)	lattice mismatch (monolayer/substrate) (%)	interlayer distance (Å)	interlayer interaction energy (eV/atom)
group IV	graphene (planar)	$(4 \times 4/2\sqrt{3} \times \sqrt{3}\ R\ 30°)$	4.8	3.1	−0.05
	silicene (buckled)	$(4 \times 4/3\sqrt{3} \times \sqrt{3}\ R\ 30°)$	1.1	2.2	−0.19
	germanene (buckled)	$(4 \times 4/3\sqrt{3} \times \sqrt{3}\ R\ 30°)$	3.2	2.2	−0.20
	stanene (buckled)	$(2 \times 2/3 \times 3)$	2.7	2.3	−0.23
group V	phosphorene (buckled)	$(3 \times 3/2\sqrt{3} \times \sqrt{3}\ R\ 30°)$	5.0	2.4	−0.11
	arsenene (buckled)	$(3 \times 3/2\sqrt{3} \times \sqrt{3}\ R\ 30°)$	4.7	2.5	−0.11
	antimonene (planar)	$(1 \times 1/1\sqrt{3} \times \sqrt{3}\ R\ 30°)$	4.1	2.7	−0.21
	bismuthene (buckled)	$(3 \times 3/4 \times 4)$	4.4	2.7	−0.17

previously reported DFT calculations find a lattice mismatch of 0.997% for silicene,[22] 3.7% for germanene,[23] and 4.38% for stanene.[45] In group V, the lattice mismatch was reported to be 6.4% for phosphorene[18] and 4.7% for aresenene.[19] For antimonene, our calculated value is different from the previously reported value[20] due to the use of the van der Waals functional D2 term in our calculations. Moreover, the substrate-supported monolayers are predicted to be stable with the binding energy of −9.0, −4.71, −3.96, and −3.28 eV/atom for graphene, silicene, germanene, and stanine, respectively. Likewise, the binding energy for the substrate-supported group V monolayers is calculated to be −5.21, −4.6, −1.43, and −3.8 eV/atom for phosphorene, arsenene, antimonene, and bismuthene, respectively. It is worth noting that a planar configuration of antimonene was reported to be formed on Ag(111), though a buckled configuration was predicted for the pristine antimonene.[20]

The interaction strength between the substrate and monolayer in the substrate-supported configuration is calculated in terms of the interaction energy ($E_{\text{interaction}}$), which is defined as follows

$$E_{\text{interaction}} = \frac{E_{(\text{substrate-supported monolayer})} - E_{(\text{substrate})} - E_{(\text{monolayer})}}{N} \quad (3)$$

where $E_{\text{substrate-supported monolayer}}$, $E_{\text{substrate}}$, and $E_{\text{monolayer}}$ are the total energy of the substrate-supported monolayer, Ag(111) substrate, and the strained monolayer, respectively, and N is the total number of atoms in the substrate-supported configuration.

The calculated results predict $E_{\text{interaction}}$ to be negative (Figure 3 and Table 1), suggesting the stability of the substrate-supported monolayer configurations for all cases. The values vary from −0.05 to −0.23 eV, with graphene the

https://doi.org/10.1021/acsomega.3c00232
ACS Omega 2023, 8, 9614−9620

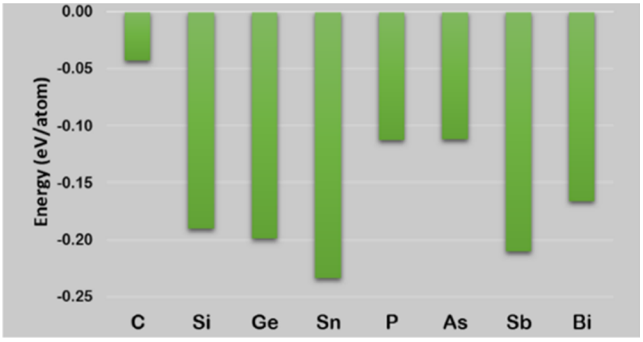

Figure 3. Calculated interaction energy between a monolayer and the Ag(111) substrate at the DFT level of theory. C, Si, Ge, Sn, P, As, Sb, and Bi represent graphene, silicene, germanene, stanene, phosphorene, arsenene, antimonene, and bismuthene, respectively.

lowest and stanene the highest. These results agree with the previously reported results, e.g., Ag(111) supported stanene.[45]

3.2. (Static) Polarizability (α) and First-Order Hyperpolarizability (β). Next, the PM7 calculations are performed to calculate static values of α and β of the pristine and their substrate-supported configurations in a finite cluster model in which monolayers were simulated by the corresponding nanoflakes. Note that the nanoflake configurations retain the structural properties obtained from the periodic DFT calculations. The edge atoms of nanoflakes are hydrogen-passivated, and a three-layer slab simulated the substrate. A (4 × 4) supercell of group-IV (or a (3 × 3) supercell of group-V) configuration was cut in such a way that the underlying substrate covers the nanoflake (Figure 4). Such a choice of construction of a nanoflake from its periodic configuration ensures its centrosymmetric nature yielding zero dipole moment and β values for the monolayers. Overall, the thickness of the substrate-supported configurations is about

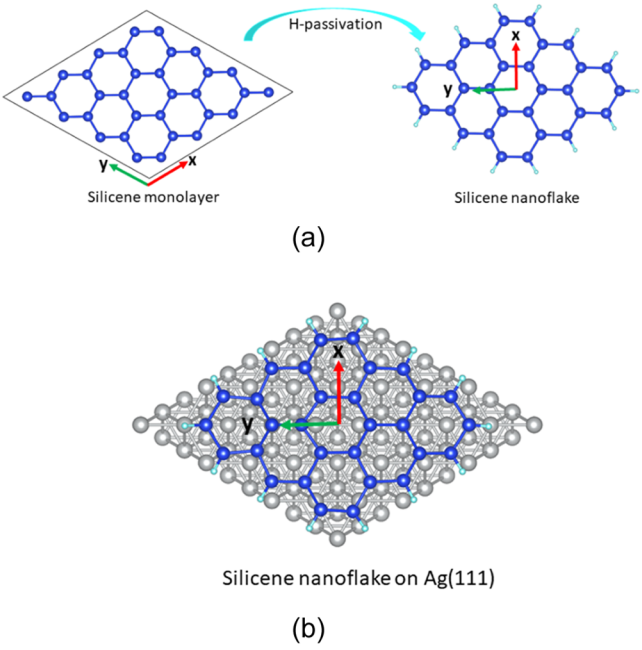

Figure 4. Schematic diagram showing the construction of nanoflakes from the equilibrium configurations of (a) periodic silicene monolayer and the corresponding nanoflake and (b) its substrate-supported configuration. Color code: Blue—Si, light blue—H, and gray—Ag.

20 Å, and C/Ag(111), Si/Ag(111), Ge/Ag(111), Sn/Ag(111), P/Ag(111), As/Ag(111), Sb/Ag(111), and Bi/Ag(111) nanoflake configurations consisted of 32/36, 32/81, 32/81, 14/57, 18/36, 18/36, 2/9, and 18/48 atoms, respectively.

A comparison of $\alpha(0)$ values calculated at the PM7 and DFT levels of theory for the pristine nanoflakes is displayed in Figure 5. We find that the PM7 results follow a similar trend in

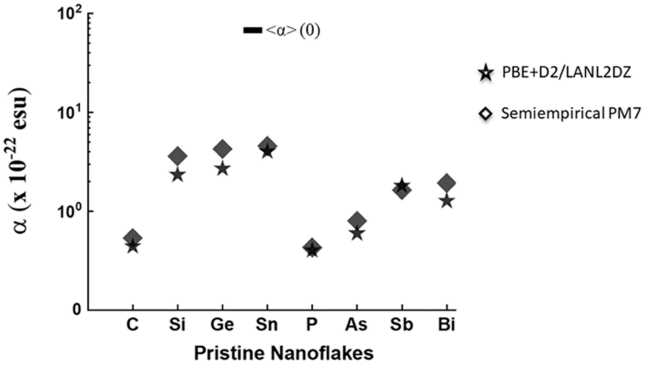

Figure 5. Comparison of DFT and PM7 calculated values α of pristine nanoflakes. β is zero due to the pristine centrosymmetric configurations of the monolayers.

static α values predicted by DFT, thereby suggesting the reliability of the PM7 results for further NLO calculations. Note that the dipole moment is zero for the pristine nanoflakes at both PM7 and DFT levels of theory, as expected.

It is well known that α is a linear property of the material, defined as the tendency of the material to acquire an electric dipole moment in proportion to an applied electric field. Here, we look into the average polarizability ($\langle\alpha\rangle$) calculated as the average of the diagonal components of the polarizability tensor given in eq 1. As the volume occupied by the electrons increases, the polarizability should generally increase, as seen in our case. This is because the electrons in a larger atom are loosely bound to those in a smaller atom. So, the polarizability increases down the group in the periodic table; hence, $\langle\alpha\rangle$ follows the trend: graphene < silicene < germanene < stanene for group-IV and phosphorene < arsenene < antimonene < bismuthene for group-V configurations (Figure 5 and Tables S2 and S3). We further note that $\langle\alpha\rangle$ may also show size dependency as the density of states increases with the number of atoms constituting a nanoflake.[46,47]

For the substrate-supported configurations, $\alpha(0)$ values are displayed in Figure 6, which are predicted to be slightly higher for the group-IV elemental monolayers (Table S4). Interestingly, the substrate-induced effects on $\alpha(0)$ do not follow the expected trend for the group-V nanoflakes, which may be due to the nature of chemical bonding at the interface, e.g., $\alpha(0)$-Sb > $\alpha(0)$-Bi. This could be attributed to the planar instead of buckled structure for antimonene interacting with the Ag(111) nanoflake.

Next, static β is determined for the substrate-supported configurations using eq 2. In the present case, the planar or buckled structure possesses centrosymmetry yielding zero dipole moments and $\beta(0)$ values. By definition, a centrosymmetric structure is one in which there exists an atom at $-x,-y,-z$ coordinates corresponding to every atom at x,y,z coordinates.

The calculated PM7 values of $\beta(0)$ of the substrate-supported configurations are displayed in Figure 6. Here, we

https://doi.org/10.1021/acsomega.3c00232
ACS Omega 2023, 8, 9614−9620

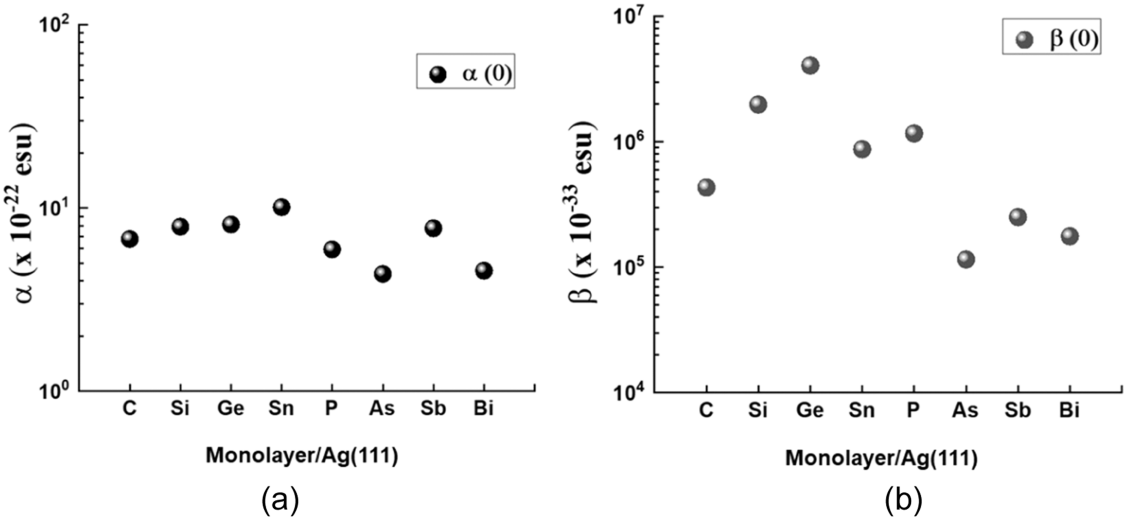

Figure 6. (a) Calculated $\alpha(0)$ and (b) $\beta(0)$ values of the substrate-supported nanoflakes. C, Si, Ge, Sn, P, As, Sb, and Bi represent graphene, silicene, germanene, stanene, phosphorene, arsenene, antimonene, and bismuthene, respectively.

find that the group IV elemental monolayers have higher $\beta(0)$ values relative to the group V elemental monolayers. For group IV, the predicted order is β (germanene) > β (silicene) > β (stanene) > β (graphene). On the other hand, the predicted order of the static values for the group-V configuration is β (phosphorene) > β (antimonene) > β (bismuthene) > β (arsenene). The predicted trend in the static first hyperpolarizabilities does not directly follow the degree of the interaction strength determined by s (Ag)−p_z (monolayer) states at the interface. Stanene (group IV) and antimonene (group V) are predicted to have a higher interaction strength with the substrate (Figure 3) but exhibit somewhat smaller β values (Figure 6b).

4. SUMMARY

The stability, equilibrium configuration, linear polarizability, α, and the first-hyperpolarizability, β, of the Ag(111)-supported monolayers (i.e., group IV (graphene, silicene, germanene, and stanene) and group V (phosphorene, antimonene, arsenene, and bismuthine)) were calculated. The periodic DFT calculations predict that all 2D monolayers considered in this study will be stable with varying degrees of interaction strength on the Ag(111) substrate surface. The monolayers interact with the Ag(111) substrate via s (Ag)−p_z (monolayer) states, and the degree of interaction depends on the nature of the p_z (monolayer) states. Calculations based using the CPHF method in the framework of the semiempirical PM7 method predict pronounced substrate-induced effects on the linear and nonlinear polarizabilities of the monolayers. The pristine monolayers possess zero dipole moment and even order NLO susceptibilities. Substrate-induced changes in the electronic density at the interface lead to significantly higher β values, which are several orders of magnitude higher than an organic molecule, such as *para*-nitroaniline.[25] This makes the substrate-supported elemental monolayers attractive candidates for next-generation photonics and integrated quantum technologies.

■ ASSOCIATED CONTENT

Supporting Information

The Supporting Information is available free of charge at https://pubs.acs.org/doi/10.1021/acsomega.3c00232.

Pristine monolayers: lattice constants calculated at PBE(DFT) + D2 level of theory (Table S1); pristine nanoflakes: polarizabilities calculated at the PM7 level of theory (Table S2); pristine nanoflakes: polarizabilities calculated at PBE(DFT) + D2 level of theory (Table S3); and substrate-supported monolayers: polarizabilities at the PM7 level of theory (Table S4) (PDF)

■ AUTHOR INFORMATION

Corresponding Authors

Ravindra Pandey − *Department of Physics, Michigan Technological University, Houghton, Michigan 49931, United States;* orcid.org/0000-0002-2126-1985; Email: pandey@mtu.edu

Shashi P. Karna − *DEVCOM Army Research Laboratory, Weapons, and Materials Research Directorate, Aberdeen, Maryland 21005-5069, United States;* Email: shashi.p.karna.civ@army.mil

Author

Sumandeep Kaur − *Department of Physics, Michigan Technological University, Houghton, Michigan 49931, United States;* Present Address: Department of Chemical Engineering, Oregon State University, Corvallis, Oregon 97331, United States

Complete contact information is available at: https://pubs.acs.org/10.1021/acsomega.3c00232

Notes

The authors declare no competing financial interest.

■ ACKNOWLEDGMENTS

The authors thank Drs. Lokanath Patra and S. Gowtham for helpful discussions. S.K. acknowledges the financial support provided by the Elizabeth and Richard Henes Center for Quantum Phenomena, Michigan Technological University. Computational resources at Michigan Technological Univer-

sity using a SUPERIOR high-performance computing cluster were utilized. The research was partially supported by the Army Research Office (ARO) through grant number W911NF-14-2-0088.

REFERENCES

(1) Lin, J. T. Nonlinear crystals for tunable coherent sources. *Opt. Quantum Electron.* **1990**, *22*, S283−S313.
(2) Meyn, J. P.; Laue, C.; Knappe, R.; Wallenstein, R.; Fejer, M. M. Fabrication of periodically poled lithium tantalate for UV generation with diode lasers. *Appl. Phys. B* **2001**, *73*, 111−114.
(3) Hagerman, M. E.; Poeppelmeier, K. R. Review of the Structure and Processing-Defect-Property Relationships of Potassium Titanyl Phosphate: A Strategy for Novel Thin-Film Photonic Devices. *Chem. Mater.* **1995**, *7*, 602−621.
(4) Castellanos-Gomez, A. Why all the fuss about 2D semiconductors? *Nat. Photonics* **2016**, *10*, 202−204.
(5) Yamashita, S. Nonlinear optics in carbon nanotube, graphene, and related 2D materials. *APL Photonics* **2019**, *4*, No. 034301.
(6) Xia, F.; Wang, H.; Xiao, D.; Dubey, M.; Ramasubramaniam, A. Two-dimensional material nanophotonics. *Nat. Photonics* **2014**, *8*, 899−907.
(7) Autere, A.; Jussila, H.; Dai, Y.; Wang, Y.; Lipsanen, H.; Sun, Z. Nonlinear Optics with 2D Layered Materials. *Adv. Mater.* **2018**, *30*, No. 1705963.
(8) Kauranen, M.; Zayats, A. V. Nonlinear plasmonics. *Nat. Photonics* **2012**, *6*, 737−748.
(9) Linden, S.; Niesler, F. B.; Forstner, J.; Grynko, Y.; Meier, T.; Wegener, M. Collective effects in second-harmonic generation from split-ring-resonator arrays. *Phys. Rev. Lett.* **2012**, *109*, No. 015502.
(10) Tsai, W. Y.; Chung, T. L.; Hsiao, H. H.; Chen, J. W.; Lin, R. J.; Wu, P. C.; Sun, G.; Wang, C. M.; Misawa, H.; Tsai, D. P. Second Harmonic Light Manipulation with Vertical Split Ring Resonators. *Adv. Mater.* **2019**, *31*, No. 1806479.
(11) Jamgotchian, H.; Colignon, Y.; Hamzaoui, N.; Ealet, B.; Hoarau, J. Y.; Aufray, B.; Biberian, J. P. Growth of silicene layers on Ag(111): unexpected effect of the substrate temperature. *J. Phys.: Condens. Matter* **2012**, *24*, No. 172001.
(12) Chiappe, D.; Grazianetti, C.; Tallarida, G.; Fanciulli, M.; Molle, A. Local electronic properties of corrugated silicene phases. *Adv. Mater.* **2012**, *24*, 5088−5093.
(13) Lin, C.-L.; Arafune, R.; Kawahara, K.; Tsukahara, N.; Minamitani, E.; Kim, Y.; Takagi, N.; Kawai, M. Structure of Silicene Grown on Ag(111). *Appl. Phys. Express* **2012**, *5*, No. 045802.
(14) Feng, B.; Ding, Z.; Meng, S.; Yao, Y.; He, X.; Cheng, P.; Chen, L.; Wu, K. Evidence of silicene in honeycomb structures of silicon on Ag(111). *Nano Lett.* **2012**, *12*, 3507−3511.
(15) Vogt, P.; De Padova, P.; Quaresima, C.; Avila, J.; Frantzeskakis, E.; Asensio, M. C.; Resta, A.; Ealet, B.; Le Lay, G. Silicene: compelling experimental evidence for graphene-like two-dimensional silicon. *Phys. Rev. Lett.* **2012**, *108*, No. 155501.
(16) d'Acapito, F.; Torrengo, S.; Xenogiannopoulou, E.; Tsipas, P.; Marquez Velasco, J.; Tsoutsou, D.; Dimoulas, A. Evidence for Germanene growth on epitaxial hexagonal (h)-AlN on Ag(1 1 1). *J. Phys.: Condens. Matter* **2016**, *28*, No. 045002.
(17) Yuhara, J.; Fujii, Y.; Nishino, K.; Isobe, N.; Nakatake, M.; Xian, L.; Rubio, A.; Lay, G. L. Large area planar stanene epitaxially grown on Ag(111). *2D Mater.* **2018**, *52*, No. 025002.
(18) Yang, S.; Hu, Z.; Wang, W.; Cheng, P.; Chen, L.; Wu, K. Regular Arrangement of Two-Dimensional Clusters of Blue Phosphorene on Ag(111). *Chin. Phys. Lett.* **2020**, *37*, No. 096803.
(19) Shah, J.; Wang, W.; Sohail, H. M.; Uhrberg, R. G. Experimental evidence of monolayer arsenene: an exotic 2D semiconducting material. *2D Mater.* **2020**, *7*, No. 025013.
(20) Shao, Y.; Liu, Z. L.; Cheng, C.; Wu, X.; Liu, H.; Liu, C.; Wang, J. O.; Zhu, S. Y.; Wang, Y. Q.; Shi, D. X.; Ibrahim, K.; Sun, J. T.; Wang, Y. L.; Gao, H. J. Epitaxial Growth of Flat Antimonene Monolayer: A New Honeycomb Analogue of Graphene. *Nano Lett.* **2018**, *18*, 2133−2139.
(21) Guo, Y.; Pan, F.; Ye, M.; Sun, X.; Wang, Y.; Li, J.; Zhang, X.; Zhang, H.; Pan, Y.; Song, Z.; Yang, J.; Lu, J. Monolayer bismuthene-metal contacts: a theoretical study. *ACS Appl. Mater. Interfaces* **2017**, *9*, 23128−23140.
(22) Curcella, A.; Bernard, R.; Borensztein, Y.; Resta, A.; Lazzeri, M.; Prévot, G. Structure and stability of silicene on Ag (111) reconstructions from grazing incidence x-ray diffraction and density functional theory. *Phys. Rev. B: Condens. Matter Mater. Phys.* **2019**, *99*, No. 205411.
(23) Lin, C. H.; Huang, A.; Pai, W. W.; Chen, W. C.; Chen, T. Y.; Chang, T. R.; Yukawa, R.; Cheng, C. M.; Mou, C. Y.; Matsuda, I.; Chiang, T. C.; et al. Single-layer dual germanene phases on Ag (111). *Phys. Rev. Mater.* **2018**, *2*, No. 024003.
(24) Zhang, K.; Sciacca, D.; Coati, A.; Bernard, R.; Borensztein, Y.; Diener, P.; Grandidier, B.; Lefebvre, I.; Derivaz, M.; Pirri, C.; Prévot, G. Resolving the structure of the striped Ge layer on Ag (111): Ag 2 Ge surface alloy with alternate fcc and hcp domains. *Phys. Rev. B: Condens. Matter Mater. Phys.* **2021**, *104*, No. 155403.
(25) Stewart, J. J. P. Optimization of parameters for semiempirical methods VI: more modifications to the NDDO approximations and re-optimization of parameters. *J. Mol. Model.* **2013**, *19*, 1−32.
(26) Hostaš, J.; Řezáč, J.; Hobza, P. On the performance of the semiempirical quantum mechanical PM6 and PM7 methods for noncovalent interactions. *Chem. Phys. Lett.* **2013**, *568*−*569*, 161−166.
(27) Kaur, S.; Pandey, R.; Karna, S. P. Enhanced nonlinear optical response of graphene-based nanoflake van der Waals heterostructures. *RSC Adv.* **2021**, *11*, 5590−5600.
(28) Kresse, G.; Furthmüller, J. Efficient iterative schemes for ab initio total-energy calculations using a plane-wave basis set. *Phys. Rev. B: Condens. Matter Mater. Phys.* **1996**, *54*, 169−186.
(29) Blöchl, P. E. Projector augmented-wave method. *Phys. Rev. B* **1994**, *50*, 17953−17979.
(30) Grimme, S. Semiempirical GGA-type density functional constructed with a long-range dispersion correction. *J. Comput. Chem.* **2006**, *27*, 1787−1799.
(31) Gao, J.; Zhao, J. Initial geometries, interaction mechanism and high stability of silicene on Ag(111) surface. *Sci. Rep.* **2012**, *2*, No. 861.
(32) Artyukhov, V. I.; Hao, Y.; Ruoff, R. S.; Yakobson, B. I. Breaking of symmetry in graphene growth on metal substrates. *Phys. Rev. Lett.* **2015**, *114*, No. 115502.
(33) Karna, S. P.; Dupuis, M. Frequency dependent nonlinear optical properties of molecules: Formulation and implementation in the HONDO program. *J. Comput. Chem.* **1991**, *12*, 487−504.
(34) Frisch, M. J.; Trucks, G. W.; Schlegel, H. B.; Scuseria, G. E.; Robb, M. A.; Cheeseman, J. R.; Scalmani, G.; Barone, V.; Petersson, G. A.; Nakatsuji, H.; Li, X.; Caricato, M.; Marenich, A. V.; Bloino, J.; Janesko, B. G.; Gomperts, R.; Mennucci, B.; Hratchian, H. P.; Ortiz, J. V.; Izmaylov, A. F.; Sonnenberg, J. L.; Williams-Young, D.; Ding, F.; Lipparini, F.; Egidi, F.; Goings, J.; Peng, B.; Petrone, A.; Henderson, T.; Ranasinghe, D.; Zakrzewski, V. G.; Gao, J.; Rega, N.; Zheng, G.; Liang, W.; Hada, M.; Ehara, M.; Toyota, K.; Fukuda, R.; Hasegawa, J.; Ishida, M.; Nakajima, T.; Honda, Y.; Kitao, O.; Nakai, H.; Vreven, T.; Throssell, K.; Montgomery, J. A., Jr.; Peralta, J. E.; Ogliaro, F.; Bearpark, M. J.; Heyd, J. J.; Brothers, E. N.; Kudin, K. N.; Staroverov, V. N.; Keith, T. A.; Kobayashi, R.; Normand, J.; Raghavachari, K.; Rendell, A. P.; Burant, J. C.; Iyengar, S. S.; Tomasi, J.; Cossi, M.; Millam, J. M.; Klene, M.; Adamo, C.; Cammi, R.; Ochterski, J. W.; Martin, R. L.; Morokuma, K.; Farkas, O.; Foresman, J. B.; Fox, D. J. *Gaussian 16*, revision C.01; Wallingford, CT, 2016.
(35) Daul, C. A.; Ciofini, I.; Weber, V. Investigation of NLO properties of substituted (M)-tetrathia-[7]-helicenes by semiempirical and DFT methods. *Int. J. Quantum Chem.* **2003**, *91*, 297−302.
(36) Praveen, P. A.; Babu, R. R.; Ramamurthi, K. Validation of PM6 & PM7 semiempirical methods on polarizability calculations. *AIP Conf. Proc.* **2015**, *1665*, No. 090011.

https://doi.org/10.1021/acsomega.3c00232
ACS Omega 2023, 8, 9614−9620

(37) Cahangirov, S.; Topsakal, M.; Akturk, E.; Sahin, H.; Ciraci, S. Two- and one-dimensional honeycomb structures of silicon and germanium. *Phys. Rev. Lett.* **2009**, *102*, No. 236804.
(38) Broek, B. v. d.; Houssa, M.; Scalise, E.; Pourtois, G.; Afanas'ev, V. V.; Stesmans, A. Two-dimensional hexagonal tin: ab-initio geometry, stability, electronic structure and functionalization. *2D Mater.* **2014**, *1*, No. 021004.
(39) Khan, I.; Son, J.; Hong, J. Metal adsorption on monolayer blue phosphorene: A first-principles study. *Phys. Lett. A* **2018**, *382*, 205−209.
(40) Kamal, C.; Ezawa, M. Arsenene: Two-dimensional buckled and puckered honeycomb arsenic systems. *Phys. Rev. B: Condens. Matter Mater. Phys.* **2015**, *91*, No. 085423.
(41) Wang, G.; Pandey, R.; Karna, S. P. Atomically thin group V elemental films: theoretical investigations of antimonene allotropes. *ACS Appl. Mater. Interfaces* **2015**, *7*, 11490.
(42) Gui, G.; Li, J.; Zhong, J. Band structure engineering of graphene by strain: First-principles calculations. *Phys. Rev. B: Condens. Matter Mater. Phys.* **2008**, *78*, No. 075435.
(43) Aktürk, E.; Aktürk, O. Ü.; Ciraci, S. Single and bilayer bismuthene: Stability at high temperature and mechanical and electronic properties. *Phys. Rev. B: Condens. Matter Mater. Phys.* **2016**, *94*, No. 014115.
(44) Ai, M.; Sun, J.; Li, Z.; Liang, H.; Liu, C. Mechanisms and Properties of Bismuthene and Graphene/Bismuthene Heterostructures as Anodes of Lithium-/Sodium-Ion Batteries by First-Principles Study. *J. Phys. Chem. C* **2021**, *125*, 11391−11401.
(45) Guo, Y.; Pan, F.; Ye, M.; Wang, Y.; Pan, Y.; Zhang, X.; Li, J.; Zhang, H.; Lu, J. Interfacial properties of stanene−metal contacts. *2D Mater.* **2016**, *3*, No. 035020.
(46) Deng, H.; Manrique, D. Z.; Chen, X.; Panoiu, N. C.; Ye, F. Quantum mechanical analysis of the nonlinear optical response of interacting graphene nanoflakes. *APL Photonics* **2018**, *3*, No. 016102.
(47) Schwerdtfeger, P.; Nagle, J. K. Table of static dipole polarizabilities of the neutral elements in the periodic table. *Mol. Phys.* **2018**, *117*, 1200−1225.

https://doi.org/10.1021/acsomega.3c00232
ACS Omega 2023, 8, 9614−9620